Investigation of energy dissipation due to contact angle hysteresis in capillary effect

Bhagya Athukorallage[1] **and Ram Iyer**[2]
Department of Mathematics and Statistics, Texas Tech University.
E-mail: bhagya.athukorala@ttu.edu[1] and ram.iyer@ttu.edu[2]

Abstract. Capillary action or Capillarity is the ability of a liquid to flow in narrow spaces without the assistance of, and in opposition to, external forces like gravity. Three effects contribute to capillary action, namely, adhesion of the liquid to the walls of the confining solid; meniscus formation; and low Reynolds number fluid flow. We investigate the dissipation of energy during one cycle of capillary action, when the liquid volume inside a capillary tube first increases and subsequently decreases while assuming quasi-static motion. The quasi-static assumption allows us to focus on the wetting phenomenon of the solid wall by the liquid and the formation of the meniscus. It is well known that the motion of a liquid on an non-ideal surface involves the expenditure of energy due to contact angle hysteresis. In this paper, we derive the equations for the menisci and the flow rules for the change of the contact angles for a liquid column in a capillary tube at a constant temperature and volume by minimizing the Helmholtz free energy using calculus of variations. We describe the numerical solution of these equations and present results from computations for the case of a capillary tube with 1 mm diameter.

1. Introduction

Capillarity and wetting phenomena play prominent roles in soil science, plant biology, surface physics, and hence, both fields gain more attention from researchers in various areas like chemistry, physics, and engineering. Studies on wetting phenomenon mainly look at how liquid spreads on a solid surface. Industrial processes, such as cleaning, painting, coating, and adhesion [1] widely use the key concepts of wetting. As an example, in the automobile industry, surfaces are prepared prior to painting, and tires are treated to promote adhesion on wet roadways.

The surface chemistry of a solid substrate is the key factor in determining its wetting behavior; hence, the specific wetting properties can be obtained by modifying the surface chemistry. At large scales, research on wetting properties of a liquid is used to increase the deposition efficiency of pesticides on plant leaves and the cooling of industrial reactors. On smaller scales, it is used to improve the efficiency of microfluidic and nanoprinting devices [2].

Capillarity is the study of the interface between two immiscible fluids, or between liquid and air. These interfaces change their shape to minimize the surface energy [3]. The two fundamental equations that describe the *macroscopic* theory of capillary surfaces are the Young-Laplace equation and the Kelvin equation. The wetting of a solid surface by a liquid in the presence of vapor is described by Young's equation [4].

- The Young-Laplace equation describes the shape of a capillary interface. When a curved capillary interface is in equilibrium, a pressure difference, δp, forms across the interface. Young-

Laplace equation relates the pressure deficiency to the curvature of the interface, and it reads

$$\delta p = 2\gamma_{LG} H, \tag{1}$$

where H denotes the mean curvature of the interface [3].

- Lord Kelvin's equation describes the evaporation or condensation of liquid from a capillary surface. In particular, this equation describes the change in the pressure of the vapor as a function of the temperature. This change in the vapor pressure leads to a change in the shape of the capillary surface in accordance with the Young-Laplace equation.
- Young's equation describes the boundary condition at the three phase line where a capillary surface meets a solid surface.
  Consider a liquid drop on a solid substrate, where one encounters three different interfaces: solid-liquid (SL), solid-gas (SG), and liquid-gas (LG). We assume that the contact line is a differentiable function so that one may assign a tangent direction at any point. We also assume that the solid and liquid surfaces are differentiable so that we may assign normal directions at any point. The *contact angle* θ between the solid and the liquid is defined to be (please refer to Figure 1) as the angle between the normal vectors to the solid and the liquid at a point on the contact line [5].

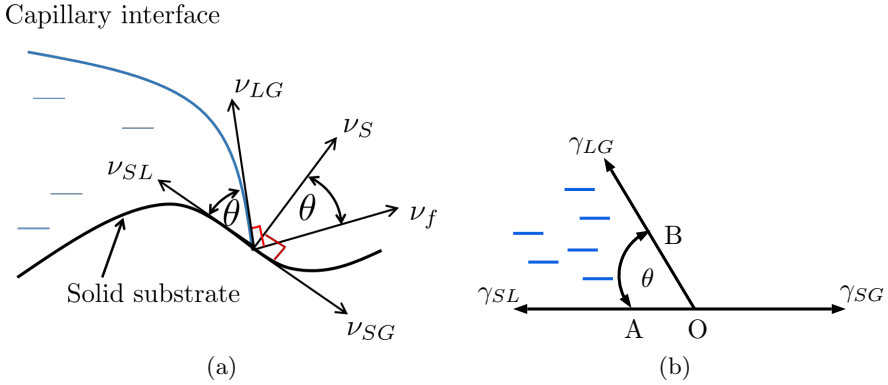

Figure 1: (a) Geometric definition of the contact angle for a 3-D droplet on a solid substrate [5]: ν_S is the normal to the solid substrate at the contact line, and ν_f is the normal to the droplet surface at the contact line. The angle between ν_S and ν_f is the contact angle. On the tangent plane to the solid substrate, let ν_{SG} be the unit vector perpendicular to the contact line pointing away from the wetted region. The vector $\nu_{SL} = -\nu_{SG}$ is the unit vector pointing into the wetted region. On the tangent plane to the capillary interface at the contact point, let ν_{LG} be the unit vector perpendicular to the contact line pointing away from the solid. (b) Forces per unit length of magnitude γ_{SG}, γ_{SL}, and γ_{LG} respectively act along the unit directions ν_{SG}, ν_{SL}, and ν_{LG}. Force balance in the ν_{SG} direction yields the Young equation.

Forces per unit length of magnitude γ_{SL}, γ_{SG}, and γ_{LG} act along certain directions perpendicular to the contact line as described in Figure 1(b). Balancing the forces on the tangent plane to the solid surface yields Young's equation [3]:

$$\gamma_{SG} - \gamma_{SL} = \gamma_{LG} \cos\theta. \tag{2}$$

The contact angle, θ, is not simply the tangential angle at the point of contact. In the region of the triple-point line (the line of contact between the substrate, air, and liquid), the liquid exhibits three distinct regions: the molecular region, the transition region, and the capillary

region [6]. It is at the transition region where one should measure the angle of contact. The angle that the transition region makes with the substrate is the contact angle to be used in the Young's law [7]. This subtlety in the notion of the contact angle will be important in Section 2.2. The scalar quantities γ_{SL}, γ_{SG}, and γ_{LG} can also be understood as the energies of the interfaces per unit area.

In this article, we continue the work presented in [8] and compute the energy that must be expended by an external agent while changing the volume of a liquid column in a capillary tube through one cycle. The liquid volume itself could be changed slowly by changing the temperature of the system through Kelvin's effect described earlier. The very fact that a liquid column exists in a vertical capillary tube implies that the angles at the upper and lower menisci have different contact angle values. This is only possible due to the contact angle hysteresis phenomenon described next.

1.1. Contact angle hysteresis

Consider a liquid droplet on a solid surface with a contact angle of θ (Fig. 2). Experiments show that if the liquid is carefully added to the droplet via a syringe, the volume and contact angle of the droplet will increase without changing its initial contact area. Further increase of its volume results in an increase in the contact area with the contact angle fixed at θ_A (refer to Fig. 2(a)). Similarly, if the liquid is removed from a droplet, volume and contact angle of the droplet decrease but retain the same contact area. Continuing this process results in a recession of the contact area at a contact angle of θ_R. These two limiting values, θ_A and θ_R, are referred to as *advancing* and *receding angles*. For a symmetric droplet, one can obtain a hysteresis diagram for the contact angle θ verses droplet diameter D as depicted in Figure 2 (b).

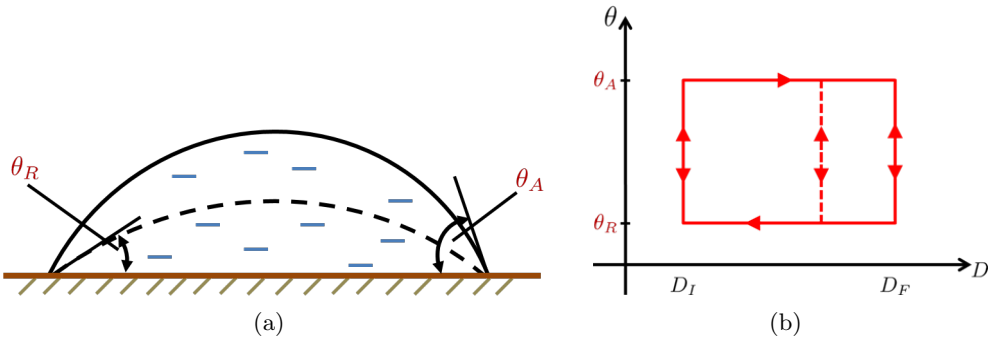

Figure 2: (a) Contact angle hysteresis effect: advancing θ_A, and receding θ_R contact angles of a liquid drop. (b) Plot of the contact angle θ verses contact diameter D for a drop on a solid surface.

1.2. Effect of surface chemistry and roughness

The contact angle θ at the contact line may be found by solving (2). It has been known since the work of H. L. Sulman and H. Picard [9] that there is a difference in the contact angle at the solid-liquid-gas contact line between rising drops and falling drops. They called this phenomenon *contact angle hysteresis*. The amount of hysteresis depends on the chemical compositions of the solid and the liquid, and the physical roughness of the solid surface [10]. Several researchers have shown that even for solids with surface height variation in the nanometers and drop sizes that are 2 or 3 orders of magnitude larger, there is still significant contact angle hysteresis [11, 12, 13, 14]. These results show that the solid-liquid chemistry is the primary reason for contact angle hysteresis. The same experiments have also shown that increase of surface roughness changes the amount of contact angle hysteresis but in a consistent manner [10, 15].

As experiments have pointed out that the primary reason for contact angle hysteresis is the chemistry between the solid and liquid, the practice of assigning only a single value for the interfacial energy γ_{SL} was questioned by Penn and Miller [12]. Recently, Snoeijer and Andreotti [16] have shown through a theoretical analysis at the microscopic level of a liquid drop on a smooth surface with no surface roughness and with no chemical impurities that the macroscopic (or apparent) contact angle cannot have a single value. Extrand[17] started with the assumption that the advancing and receding contact angles are known and concluded that the interfacial energy of the solid-liquid must be set valued if the angles are different.

Due to the above mentioned reasons, we assume γ_{SL} takes values in the set $[\gamma_{SL_{\min}}, \gamma_{SL_{\max}}]$. In the next section, we follow the theory outlined in [8] to derive the equations satisfied by a finite column of liquid in a capillary tube.

1.3. Derivation of equations

We obtain the governing equations for a capillary surface by minimizing the total energy of the three-phase system (solid-liquid-gas) in a capillary tube for a constant liquid volume and temperature, while subject that $\gamma_{SL} \in [\gamma_{SL_{\min}}, \gamma_{SL_{\max}}]$ [8]. Consider a capillary surface formed between a three-phase system: liquid, gas, and a solid boundary. Let the domain occupied by the liquid be Ω and the domain of the capillary interface be S. Further, S_w denotes the area of the wetted part of the solid boundary. The total energy of this system consists of three main terms [18]:

(i) Free surface energy,
(ii) Wetting energy, and
(iii) Gravitational potential energy.

The free surface energy, $\mathcal{E}_f$, of a capillary interface is proportional to the area of the liquid surface that is not in contact with the solid. Then, if the energy per unit area (surface tension) is γ_{LG},

$$\mathcal{E}_f = \gamma_{LG} \int_S dS. \tag{3}$$

In equation (3), dS represents the surface area element on the capillary interface. In equation (4), wetting energy, $\mathcal{E}_w$, is the adhesion energy between the liquid and the solid substrate, and

$$\mathcal{E}_w = \int_{S_w} (\gamma_{SL} - \gamma_{SG})\, dS_w. \tag{4}$$

Note that in this quantity, γ_{SL} is not a constant function. Finally, the gravitational potential energy, $\mathcal{E}_g$, in terms of the height coordinate z and volume element dV is

$$\mathcal{E}_g = \int_\Omega \rho g\, z\, dV, \tag{5}$$

where ρ and g are the liquid density and gravitational acceleration, respectively. The total Helmholtz energy at constant temperature of the system is then given by:

$$\mathcal{E}_{tot} = \mathcal{E}_f + \mathcal{E}_w + \mathcal{E}_g. \tag{6}$$

One obtains equations for the capillary surfaces and the boundary conditions at the contact line from first-order necessary conditions arising from the minimization of the total energy functional subject to a constant liquid volume constraint and $\gamma_{SL} \in [\gamma_{SL_{\min}}, \gamma_{SL_{\max}}]$.

2. Liquid column in a capillary tube: Effect due to the contact angle hysteresis

Experiments suggest that a thin, vertical capillary can hold a finite column of liquid. Consider a liquid column trapped in a capillary tube with radius R. Let θ_1 and θ_2 be the equilibrium contact angles of the upper and lower menisci, respectively. Hence, for the static equilibrium of the liquid column, it satisfies the equation:

$$2\pi R\gamma_{LG}(\cos\theta_1 - \cos\theta_2) = \rho\, g\, V, \tag{7}$$

where γ_{LG} is the interfacial tension between the liquid-gas interface, and ρ, V denote the density and volume of the liquid respectively. Thus, the existence of such a capillary column implies that the equilibrium contact angles θ_1 and θ_2 satisfy $\theta_1 < \theta_2$.

Given V, to find the angles θ_1 and θ_2, we mathematically model the capillary menisci formed in a liquid column trapped in a cylindrical tube. As our goal is to find concrete values for energy losses for comparison purposes, we restrict ourselves to the case where the capillary interface is axisymmmetric. Governing equations for the upper and lower menisci are obtained using calculus of variations [18, 19, 20] after minimizing the total energy functional at a constant temperature subject to the constraint that $\gamma_{SL} \in [\gamma_{SL_{\min}}, \gamma_{SL_{\max}}]$.

Consider an axisymmetric capillary column in a tube with radius R. Let the liquid density be ρ. The profiles of the upper and lower menisci are $h_1(r)$ and $h_2(r)$ with contact angles θ_1 and θ_2, respectively. Consider the Cartesian coordinate system as depicted in Figure 3. The distance between the origin with the minimum of the upper meniscus and maximum of the lower meniscus are H_1 and H_2; $\bar{p}_0$ is the capillary pressure at the origin, and $\bar{p}_0 \equiv p(0) - p_{atm}$. Interfacial tensions between the solid-gas, solid-liquid, and liquid-gas are γ_{SG}, γ_{SL}, and γ_{LG}.

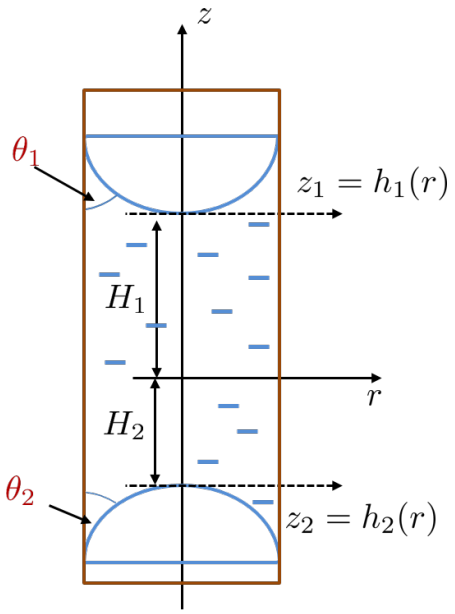

Figure 3: Schematic drawing of a liquid column in a capillary tube with gravity acting along the $-z$ direction. Upper and lower contact angles satisfy $\theta_1 < \theta_2$. The capillary surface heights $z_i = h_i(r)$, $i = 1, 2$ are measured from the base of the surface as shown in figure with z direction as positive – hence, h_2 is a non-positive function whilst h_1 is a non-negative function.

Let the total surface area of the tube be A_t. The total energy functional, $\mathcal{E}_{tot}$, is

$$\begin{aligned}\mathcal{E}_{tot} &= \left(A_t - 2\pi R \int_{H_2+h_2(R)}^{H_1+h_1(R)} dz\right)\gamma_{SG} + 2\pi R \int_{H_2+h_2(R)}^{H_1+h_1(R)} \gamma_{SL}(z)\, dz + \\ &\gamma_{LG} \int_0^R 2\pi r \sqrt{1+h_1'^2(r)}\, dr + \gamma_{LG} \int_0^R 2\pi r \sqrt{1+h_2'^2(r)}\, dr + \\ &\int_0^R \int_{H_2+h_2(r)}^{H_1+h_1(r)} 2\pi r\, \rho g\, z\, dz\, dr. \end{aligned} \tag{8}$$

In (8), the first two terms are the energy contribution due to the non-wetting and wetting surfaces, on the capillary tube, respectively. These two energy terms are described by the integrals over the wetting and non-wetting area of the capillary tube. In the second term, γ_{SL} takes values in the interval $[\gamma_{SL_{\min}}, \gamma_{SL_{\max}}]$ and it is considered to be z-dependent. The third and the fourth terms describe the capillary surface energy of the upper and lower meniscus profiles. This energy term is related to the capillary-free surface area. Gravitational potential energy term is represented by the last term and is defined over the liquid volume; liquid density is ρ, and g is the gravitational acceleration.

Expression (8) may be simplified to

$$\begin{aligned}\mathcal{E}_{tot} &= A_t\gamma_{SG} + 2\pi R \int_{H_2+h_2(R)}^{H_1+h_1(R)} (\gamma_{SL}(z) - \gamma_{SG})\, dz + \gamma_{LG} \int_0^R 2\pi r \sqrt{1+h_1'^2(r)}\, dr + \\ &\gamma_{LG} \int_0^R 2\pi r \sqrt{1+h_2'^2(r)}\, dr + 2\pi\rho g \int_0^R \frac{r}{2}[(h_1(r)+H_1)^2 - (h_2(r)+H_2)^2]\, dr. \end{aligned} \tag{9}$$

2.1. Derivation of the equilibrium conditions: First variation of the total energy functional
By minimizing the total energy of the system at constant volume and temperature subject to the constraint $\gamma_{SL} \in [\gamma_{SL_{\min}}, \gamma_{SL_{\max}}]$, we find the equilibrium meniscus profiles: $h_1(r)$ and $h_2(r)$ and the liquid column heights: H_1 and H_2. This approach results in the associated Euler-Lagrange equation for $h_1(r)$, $h_2(r)$, H_1, and H_2 together with the boundary conditions at the three-phase contact line [21, 18, 22]. These boundary conditions yield the corresponding Young's equation at the upper and lower contact lines. Furthermore, we also obtain flow rules for the change in the contact angles when the contact lines move.

Although volume V is considered to be constant, the wetting area is allowed to vary, and therefore, we take the first variation of (9) with respect to the variables: H_1, H_2, $h_1(r)$, and $h_2(r)$. Denote the Lagrange multiplier corresponding to the constant volume constraint as $\bar{p}$. Then,

$$\begin{aligned}\delta\mathcal{E}_{tot} - \bar{p}\,\delta\,V &= 2\pi R[\gamma_{SL}(H_1 + h_1(R)) - \gamma_{SG}](\delta H_1 + \delta h_1(R)) - \\ &\quad 2\pi R[\gamma_{SL}(H_2 + h_2(R)) - \gamma_{SG}](\delta H_2 + \delta h_2(R)) + \\ &\quad \gamma_{LG}\int_0^R 2\pi r\left[\frac{h_1'(r)}{\sqrt{1+h_1'^2(r)}}\delta h_1' + \frac{h_2'(r)}{\sqrt{1+h_2'^2(r)}}\delta h_2'\right]dr + \\ &\quad 2\pi\rho g\int_0^R r[(h_1(r)+H_1)(\delta h_1(r)+\delta H_1) - (h_2(r)+H_2)(\delta h_2(r)+\delta H_2)]\,dr - \\ &\quad 2\pi\bar{p}\int_0^R r[\delta h_1(r) + \delta H_1 - \delta h_2(r) - \delta H_2]\,dr \\ &\leq 0, \end{aligned} \tag{10}$$

where the inequality is due to the fact that equality may not be attained due to the constraint $\gamma_{SL} \in [\gamma_{SL_{\min}}, \gamma_{SL_{\max}}]$. By using integration by parts, the first integral in (10) may be recast into

$$\int_0^R r\frac{h_i'(r)}{\sqrt{1+h_i'^2(r)}}\delta h_i'\,dr = r\frac{h_i'(r)}{\sqrt{1+h_i'^2(r)}}\delta h_i(r)\Big|_0^R - \int_0^R\left(\frac{rh_i'(r)}{\sqrt{1+h_i'^2(r)}}\right)'\delta h_i(r)\,dr \quad \text{for } i \in \{1,2\}, \tag{11}$$

and hence, (10) can be rewritten in the form:

$$\begin{aligned}\delta\mathcal{E}_{tot} - \bar{p}\,\delta\,V &= R[\gamma_{SL}(H_1 + h_1(R)) - \gamma_{SG}](\delta H_1 + \delta h_1(R)) - \\ &\quad R[\gamma_{SL}(H_2 + h_2(R)) - \gamma_{SG}](\delta H_2 + \delta h_2(R)) + \\ &\quad \gamma_{LG}\frac{rh_1'(r)}{\sqrt{1+h_1'^2(r)}}\delta h_1(r)\Big|_0^R + \gamma_{LG}\frac{rh_2'(r)}{\sqrt{1+h_2'^2(r)}}\delta h_2(r)\Big|_0^R - \\ &\quad \gamma_{LG}\int_0^R\left(\frac{rh_1'(r)}{\sqrt{1+h_1'^2(r)}}\right)'\delta h_1(r)\,dr - \gamma_{LG}\int_0^R\left(\frac{rh_2'(r)}{\sqrt{1+h_2'^2(r)}}\right)'\delta h_2(r)\,dr + \\ &\quad \rho g\int_0^R r[(h_1(r)+H_1)(\delta h_1(r)+\delta H_1) - (h_2(r)+H_2)(\delta h_2(r)+\delta H_2)]\,dr - \\ &\quad \bar{p}\int_0^R r[\delta h_1(r) + \delta H_1 - \delta h_2(r) - \delta H_2]\,dr. \end{aligned} \tag{12}$$

The necessary condition for $\mathcal{E}_{tot}$ to have an extremum is $\delta\mathcal{E}_{tot} - \bar{p}\,\delta V \leq 0$. Now, $\delta\,h_1(r)$ and $\delta\,h_2(r)$ have no restriction on sign and so we get:

$$-\gamma_{LG}\left(\frac{rh_1'(r)}{\sqrt{1+h_1'^2(r)}}\right)' - \bar{p}\,r + \rho g r(h_1(r)+H_1) = 0, \tag{13}$$

$$-\gamma_{LG}\left(\frac{rh_2'(r)}{\sqrt{1+h_2'^2(r)}}\right)' + \bar{p}\,r - \rho g r(h_2(r)+H_2) = 0. \tag{14}$$

Similarly, δH_1 and δH_2 have no restriction on sign and this leads to:

$$\Big(\gamma_{SL}(H_1+h_1(R))-\gamma_{SG}\Big)R - \bar{p}\,\frac{R^2}{2} + \rho g\int_0^R rh_1(r)\,dr + \rho g H_1\frac{R^2}{2} = 0, \tag{15}$$

$$-\Big(\gamma_{SL}(H_2+h_2(R))-\gamma_{SG}\Big)R + \bar{p}\,\frac{R^2}{2} - \rho g\int_0^R rh_2(r)\,dr - \rho g H_2\frac{R^2}{2} = 0. \tag{16}$$

These equations are satisfied for $r\in[0,R]$. With these deductions, the inequality $\delta\mathcal{E}_{tot}-\bar{p}\,\delta V\le 0$ reduces to:

$$\begin{aligned}\delta\mathcal{E}_{tot}-\bar{p}\,\delta V &= R[\gamma_{SL}(H_1+h_1(R))-\gamma_{SG}]\,\delta h_1(R) - R[\gamma_{SL}(H_2+h_2(R))-\gamma_{SG}]\,\delta h_2(R) + \\ &\quad \gamma_{LG}\frac{rh_1'(r)}{\sqrt{1+h_1'^2(r)}}\delta h_1(r)\Big|_0^R + \gamma_{LG}\frac{rh_2'(r)}{\sqrt{1+h_2'^2(r)}}\delta h_2(r)\Big|_0^R \\ &\le 0.\end{aligned} \tag{17}$$

Note that the contact line variation $\delta h_1(R)$ and $\delta h_2(R)$ are related to θ_1 and θ_2 respectively. For a particular θ_i value, $\delta h_i(R)$ is determined by the inequality (17). To simplify notation, denote:

$$\frac{\gamma_{SG}-\gamma_{SL}(H_1+h_1(R))}{\gamma_{LG}} = \cos\theta_{Y_1}, \tag{18}$$

$$\frac{\gamma_{SG}-\gamma_{SL}(H_2+h_2(R))}{\gamma_{LG}} = \cos\theta_{Y_2}, \tag{19}$$

Note that for $i=1,2$, $\cos\theta_{Y_i}\in[\cos\theta_A,\cos\theta_R]$. Then, using the fact that $h_1'(R)=\cot\theta_1$ and $h_2'(R)=-\cot\theta_2$, inequality (17) becomes:

$$(\cos\theta_1-\cos\theta_{Y_1})\,\delta h_1(R) + (\cos\theta_2-\cos\theta_{Y_2})\,\delta h_2(R)\le 0 \tag{20}$$

Define: $\cos\theta_A := \frac{\gamma_{SG}-\gamma_{SL_{\max}}}{\gamma_{LG}}$ and $\cos\theta_R := \frac{\gamma_{SG}-\gamma_{SL_{\min}}}{\gamma_{LG}}$. We have the following cases. For $i=1,2$,

(i) If $\cos\theta_i\in(\cos\theta_A,\cos\theta_R)$, then $\forall\,\theta_{Y_i}$, $(\cos\theta_i-\cos\theta_{Y_i})\lneqq 0$. Hence by (20) $\delta h_i(R)=0$.
(ii) If $\cos\theta_i=\cos\theta_A$, then $\forall\,\theta_{Y_i}$, $(\cos\theta_i-cos\theta_{Y_i})\le 0$. Thus, by (20) $\delta h_i(R)\ge 0$.
(iii) If $\cos\theta_i=\cos\theta_R$, then $\forall\,\theta_{Y_i}$, $(\cos\theta_i-\cos\theta_{Y_i})\ge 0$. Hence, by (20) $\delta h_i(R)\le 0$.

The above inequalities yield the *flow rules* for the contact line motion and correspond to observed results from experiment described in Section 1.1.

2.2. Concept of capillary pressure and solution of the system of equations

First, we provide a physical interpretation to the Lagrange multiplier term $\bar{p}$. The left hand side of Inequality (10) may be thought of as the first variation of the *augmented* energy functional $\mathcal{E}_{aug} = \mathcal{E}_{tot} - \bar{p}\,V$. From Equation (8), we see that the last (gravitational energy) term of $\mathcal{E}_{aug}$ is

$$\int_0^R \int_{H_2+h_2(r)}^{H_1+h_1(r)} 2\pi r\,(-\bar{p} + \rho\,g\,z)\,dz\,dr.$$

This expression allows us to interpret $\bar{p}$ as the pressure at the origin $z = 0$. We term this pressure as the *Capillary pressure*.

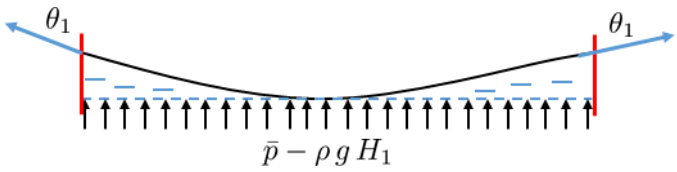

Figure 4: Schematic drawing showing the top meniscus with a liquid column underneath. Force balance on this meniscus is given by Equation (21).

Equation (15) may be rewritten after multiplication by $2\,\pi$ as:

$$\cos\theta_{Y_1}\,\gamma_{LG}\,(2\,\pi\,R) + (\bar{p} - \rho\,g\,H_1)\,(\pi\,R^2) = \rho g \int_0^R 2\,\pi\,r h_1(r)\,dr. \tag{21}$$

Equation (21) represents the balance of forces for the liquid column under the meniscus $z_1 = h_1(r)$ (see Figure 4). It is interesting to note the first term on the left hand side. As the real contact angle is θ_1, the difference $(\cos\theta_{Y_1} - \cos\theta_1)\,\gamma_{LG}\,(2\,\pi\,R)$ represents the additional force due to the adhesion between the solid wall and the liquid column – a similar or same interpretation may be found in Joanny and de Gennes [23].

Now, to facilitate computation, we make the *assumption* that the height of the liquid column under the meniscus as shown in Figure 4 is much smaller than the height of the entire liquid in the capillary tube. This assumption is a minor one and facilitates the computation of the quantities easily as we can re-state the assumption as $\theta_{Y_1} = \theta_1$. Similarly, we assume that $\theta_{Y_2} = \theta_2$ by considering the bottom meniscus. Note that, with this assumption, (18) yields: $\gamma_{SG} - \gamma_{SL}(H_1 + h_1(R)) = \gamma_{LG}\cos\theta_1$ which is Young's law applied to the contact line of the top meniscus.

Denote by $\alpha = \rho g R^2$. Solving (15) and (16) for H_1 and H_2, we get

$$H_1 = \frac{2\gamma_{LG}\cos\theta_1 R}{\alpha} + \frac{\bar{p}R^2}{\alpha} - \frac{2\rho g}{\alpha}\int_0^R r h_1(r)\,dr, \tag{22}$$

$$H_2 = \frac{2\gamma_{LG}\cos\theta_2 R}{\alpha} + \frac{\bar{p}R^2}{\alpha} - \frac{2\rho g}{\alpha}\int_0^R r h_2(r)\,dr. \tag{23}$$

Substituting H_1 from (22) into Equation (13), we obtain a partial differential equation for $h_1(r)$ that depends on the parameter $\bar{p}$. Similarly, we may obtain a partial differential equation for $h_2(r)$. We solve these PDEs using COMSOL® Multiphysics software.

2.3. Energy dissipation due to hysteresis

In [8], it is shown that the energy that must be input by an external source over the time interval $[0, T]$ for the volume to change according to the profile given by $V(t)$ (assumed to be differentiable with respect to t), where $t \in [0, T]$ is given by:

$$\mathcal{W} = \int_{t_0}^{t_f} \bar{p}(t)\, \dot{V}(t)\, dt, \tag{24}$$

where $\bar{p}(t)$ is the capillary pressure associated with the volume $V(t)$. The above formula states that if the capillary pressure $\bar{p}$ is plotted against the volume then the area of the region under the curve yields the energy input from the external source that is causing the volume to change. As the relation between $\bar{p}$ and V shows hysteresis (see Section 3), Equation (24) equivalently represents the energy loss due to contact angle hysteresis when the volume of the liquid is changed in a cycle. If the initial and final volumes are not the same, then Equation (24) also includes the internal (potential) energy change in addition to the energy loss. Although capillary effect is a complex phenomenon, it is interesting to note that the energetics of the system may be described by two scalar variables - the volume of the liquid and the capillary pressure!

In the next section, we consider a specific profile for the volume change and compute the energy that must be input by an external source to complete a cycle.

3. Numerical results and Discussion

The formation of an axisymmetric liquid column in a capillary tube is depicted in Figure 3. In the present study, we investigate the dissipation of energy during one cycle of capillary action, when the liquid volume inside the capillary tube first increases and subsequently decreases. Figure 5 shows a hysteresis diagram obtained by considering the variation of wetting area with the liquid volume. Let θ_1 and θ_2 be the upper and lower contact angle values and assume both angles are invariant along the corresponding contact lines. A_{Low} is the initial wetting area. Recall the necessary condition: $\theta_1 < \theta_2$ for the static equilibrium of the liquid column. We first consider the increase in the liquid volume at $\theta_1 = \theta_R$ and $\theta_R < \theta_2 < \theta_A$ (refer Figure 5). During this process, assume both θ_1 and θ_2 increasing until θ_2 reaches its advancing angle θ_A, and $\theta_R < \theta_1 < \theta_A$ (segment 1–2). Once θ_2 equals θ_A, further continuation of liquid addition results in a downward motion of the lower contact line with a constant contact angle θ_A and a decrease in the upper contact angle θ_1(segment 2–3). At point 3, let the wetting area be A_{High}, and θ_1 is still in the interval $[\theta_R, \theta_A]$. Paths 3–4 and 4–1 refer to the decrease in the liquid volume. As volume is quasi-statically removed, assume both θ_1 and θ_2 decrease until θ_1 approaches its receding value, and let θ_2 be in the interval $[\theta_R, \theta_A]$ at the point 4. Hence, segment 3–4 depicts a constant wetting area. Since $\theta_1 = \theta_R$, now the lower meniscus begins to recede with constant contact angle θ_R. Liquid is removed until the column arrives at the initial configuration: that is, wetting area A_{Low} and liquid volume V_1. This formulation assumes that both upper and lower contact lines be pinned during the segments 1–2 and 3–4.

On vertical segments 1–2 and 3–4 the wetting area is fixed at A_{Low} and A_{High} respectively. On segments 2–3 and 4–1, $\theta_2 = \theta_A$ and $\theta_1 = \theta_R$, respectively. Thus, we solve the governing equations (13) – (16), for the upper and lower menisci with appropriate boundary conditions (described below) using the COMSOL® Multiphysics software.

Upper and lower capillary surfaces are numerically computed by using the boundary conditions: $h_1'(0) = h_2'(0) = 0$, $h_1'(R) = \cot\theta_1$, and $h_2'(R) = -\cot\theta_2$ with prescribed θ_1 and θ_2. Additional wetting area constraint is imposed to calculate the capillary surfaces that correspond to the line segments 1–2 and 3–4. For the numerical computations, we consider capillary tubes with a diameter of 5mm and 1mm. All the numerical computations are made with $\gamma_{LG} = 73\,\mathrm{mJ/m^2}$, $\rho = 1000\,\mathrm{kg/m^3}$, and $g = 9.82\,\mathrm{m/s^2}$ [3].

Wetting area, liquid volume, and area of the upper and lower interfaces are numerically computed for each solution.

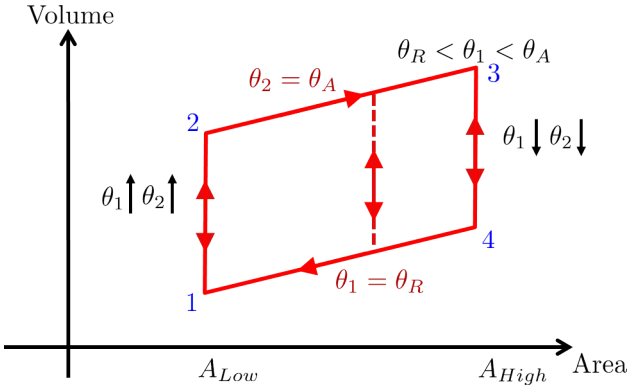

Figure 5: A hysteresis diagram for a capillary column: the liquid volume variation with respect to the wetting area of the liquid column.

Results of numerical computations of upper and lower menisci in a capillary tube of diameter $2R = 5\,\text{mm}$ are displayed in Figure 6. Upper and lower contact angles are at 35° and 65°, respectively. The liquid column volume is $4.63 \times 10^{-8}\,\text{m}^3$. For any pair of $\{\theta_1, \theta_2\}$, the volume V of the liquid may be calculated using the static equilibrium condition:

$$2\pi\gamma_{LG}R(\cos\theta_1 - \cos\theta_2) = \rho g V, \tag{25}$$

hence, we use the criterion (25) to validate our meniscus profiles.

We calculate the energy losses when the liquid volume inside the capillary tube first increases and subsequently decreases. The corresponding energy diagram is in Figures 7. Area under each closed loop denotes the energy dissipation due to the capillary pressure. Table 1 presents the variations of the energy terms for different upper and lower contact angle (θ_1 and θ_2) values.

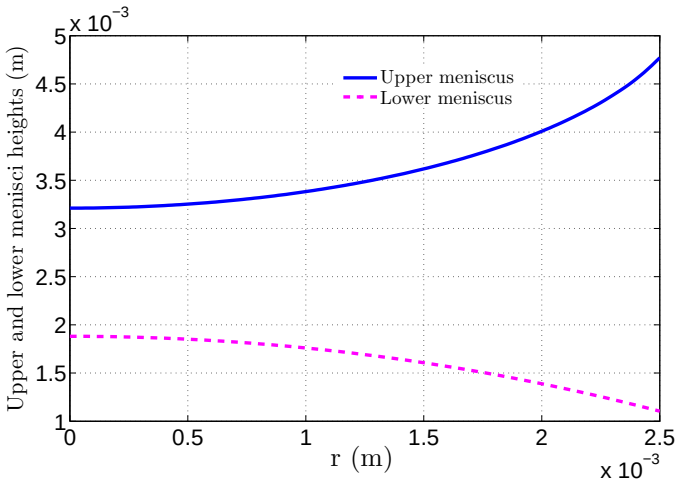

Figure 6: Upper and lower menisci profiles. The capillary tube diameter is 5mm, and the capillary pressure at the origin $\bar{p}(0) = -10\,\text{N/m}^2$. In this numerical simulation, the upper and lower contact angles are $\theta_1 = 35°$ and $\theta_2 = 65°$, respectively. The liquid bridge has the wetting area $5.76 \times 10^{-5}\,\text{m}^2$ with volume $4.63 \times 10^{-8}\,\text{m}^3$.

Table 1: Energy variations with capillary tube with diameter of 1 mm. Initial and final wetting areas are $4.00 \times 10^{-5}\,\mathrm{m}^2$ and $4.18 \times 10^{-5}\,\mathrm{m}^2$. All the numerical computations are performed under the assumptions of advancing angle $\theta_A = 66^\circ$ and receding angle $\theta_R = 30^\circ$.

θ_1	θ_2	Wetting area $\times 10^{-5}(\mathrm{m}^2)$	Volume $\times 10^{-8}(\mathrm{m}^3)$	Capillary Pressure $(\mathrm{N/m}^2)$
30.0	62.0	3.99	1.85	-7.05
30.8	62.6	4.00	1.86	-11.32
33.6	64.4	4.00	1.87	-15.28
36.0	66.0	4.00	1.88	-18.94
35.8	66.0	4.02	1.89	-18.51
35.6	66.0	4.04	1.90	-18.20
35.4	66.0	4.06	1.91	-17.88
35.2	66.0	4.08	1.92	-17.57
35.0	66.0	4.10	1.93	-17.25
34.8	66.0	4.12	1.94	-16.93
34.6	66.0	4.14	1.95	-16.62
34.2	66.0	4.18	1.97	-16.07
33.0	65.2	4.18	1.96	-14.22
31.2	64.0	4.18	1.95	-11.52
30.0	63.2	4.18	1.94	-9.6
30.0	63.0	4.13	1.93	-9.23
30.0	62.6	4.07	1.90	-8.37
30.0	62.4	4.04	1.88	-7.90

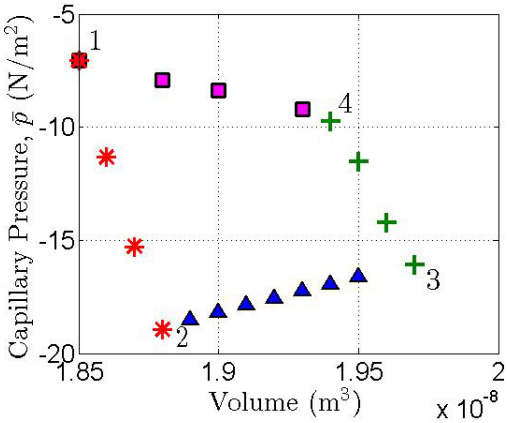

Figure 7: Energy diagram for capillary pressure versus liquid volume. Capillary tube diameter is 1 mm, and in this numerical simulation $\theta_R = 30°$ and $\theta_A = 66°$. The low and high wetting areas are 4.00×10^{-5} m^2 and 4.18×10^{-5} m^2, respectively. Energy required to complete the cycle 1–2–3–4–1 is approximately 8.21 nJ.

Table 1 shows the capillary energy variations with volume of the liquid column. Rows 1–4, 5–11, 12–15, and 16–18 of the table correspond to the volume variations that also correspond to line segments 1–2, 2–3, 3–4, and 4–1, respectively (see the hysteresis diagram: Figure 5). Figure 7 depicts the capillary pressure variation with volume of the liquid column with diameter of 1 mm. Energy required to complete the cycle 1–2–3–4–1 is approximately 8.21 nJ.

3.1. Energy losses due to viscosity of the liquid

A study of the energy mechanisms involved in wetting and drying of water in soil is very important in the field of climate change, and also for determining optimal irrigation procedures for agriculture [24]. Soil pore spaces are micro capillary tubes which fill-up and dry-out due to rainfall and/or irrigation. Completion of one cycle of wetting and drying involves motion of the contact line. There are two different mechanisms for energy lost in this process – (1) hysteresis that originates due to contact angle hysteresis, which is rate-independent; (2) viscous friction opposing fluid motion.

Numerical computation presented in Section 3 shows that the energy demand due to rate-independent hysteresis for a capillary tube with diameter of 0.1 cm, approximate wetting area of 0.4 cm^2, and capillary surface motion of 0.006 cm (corresponding to wetting area change of 0.018 cm^2) is 0.0821 ergs. Next, we consider viscous friction during contact line motion so that one may compare numbers and get an idea of the more dominant mechanism of entropy increase (or increase in internal energy of the liquid and surroundings) in capillary effect. To enable analysis, and for clarity, a simpler configuration of a liquid bridge is chosen as shown in Figure 8 for analysis [25, 26].

In the previous research work [25, 26], we investigated the viscous energy dissipation of a fluid flow that results as a consequence of the deformation of a capillary interface. In particular, we considered a capillary surface between two parallel, non-ideal solid surfaces and assumed the invariance of the interface in $z-$direction (see Figure 8). The fluid flow was analyzed using the Navier-Stokes and Continuity equations, and the viscous energy dissipation was numerically computed during the deformation of the interface. The distance between two plates is 0.1 cm and the wetting area change is approximately 0.01 cm^2. During the motion of the capillary interface, we found the energy dissipation due to viscosity to be 3.64×10^{-4} ergs. For this reason, hysteresis energy loss seems to be significantly greater (by a factor of more than 200) than energy loss due to viscosity for comparable dimensions.

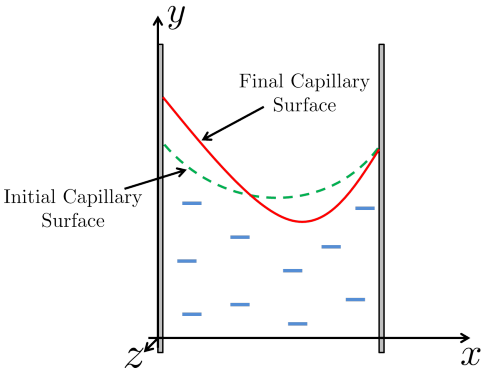

Figure 8: Two vertical plates, which are immersed in a liquid. Capillary interface is invariant in the $z-$direction.

4. Conclusions

In this study, we investigated the energy dissipation due to the effect of contact angle hysteresis using a liquid column formed in a capillary tube in which volume of the column first increases and subsequently decreases. Equations for the upper and lower menisci were obtained by minimizing the Helmholtz energy at a constant volume and temperature subject to the constraint that the energy of the interface between the solid and the liquid takes values in an interval. We present numerical solutions of the derived equations for the case of a capillary tube with 1 mm diameter. The energy required to overcome contact angle hysteresis seems to be 2 orders of magnitude greater than that required to overcome fluid viscosity for a comparable liquid bridge. This suggests that contact angle hysteresis is the dominant mechanism of energy loss in nano-fluidics.

References

[1] Extrand C W 2002 *Langmuir* **1** 7991–7999

[2] Bonn D, Eggers J, Indekeu J, Meunier J and Rolley E 2009 *Reviews of Modern Physics* **81** 739–805 ISSN 0034-6861

[3] de Gennes P G, Brochard-Wyart F and Quere D 2003 *Capillarity and Wetting Phenomena: Drops, Bubbles, Pearls, Waves* (Springer)

[4] Butt H and Kappl M 2009 *Surface and interfacial forces* (John Wiley & Sons)

[5] Alberti G and DeSimone A 2011 *Archive for rational mechanics and analysis* **202** 295–348

[6] Lin S Y, Chang H C, Lin L W and Huang P Y 1996 *Review of Scientific Instruments* **67** 2852–2858

[7] Merchant G J and Keller J B 1992 *Physics of Fluids A: Fluid Dynamics* **4** 477–485

[8] Athukorallage B, Aulisa E, Iyer R and Zhang L 2015 *Langmuir* **31** 2390–2397

[9] Sulman H L and Picard H K 1920 *The theory of concentration processes involving surface-tension* (Original typewritten notes, Columbia University, NY)

[10] de Gennes P G 1985 *Reviews Modern Physics* **57** 828–861

[11] Dettre R and Johnson Jr R 1964 Contact angle hysteresis ii: Contact angle measurements on rough surfaces *Contact Angle, Wettability, and Adhesion* ed Fowkes F (American Chemical Society) pp 136–144

[12] Penn L and Miller B 1980 *Journal of Colloid and Interface Science* **1** 238–241

[13] Ramos S, Charlaix E and Benyagoub A 2003 *Surface Science* **540** 355–362

[14] Chibowski E and Malgorzata J 2013 *Colloid Polymer Science* **291** 391–399

[15] Marmur A 2010 A guide to the equilibrium contact angles maze *Contact Angle, Wettability, and Adhesion* ed Mittal K L (Brill, Leiden) pp 3–18

[16] Snoeijer J and Andreotti B 2008 *Physics of Fluids* **20** 057101

[17] Extrand C W 1998 *Journal of Colloid and Interface Science* **207** 11–19

[18] Finn R 1986 *Equilibrium capillary surfaces* (Springer-Verlag)

[19] Frankel T 1997 *The Geometry of Physics: An Introduction* (Cambridge University Press) ISBN 9780521383349

[20] Evans L 2010 *Partial Differential Equations* Graduate studies in mathematics (American Mathematical Society) ISBN 9780821849743

[21] Bullard J W and Garboczi E J 2009 *Phys. Rev. E* **79**(1) 011604

[22] Gelfand I and Fomin S 2000 *Calculus of Variations* (Dover Publications)

[23] Joanny J F and de Gennes P G 1984 *The Journal of Chemical Physics* **81** 552–562 ISSN 00219606

[24] Appelbe B, Flynn D, McNamara H, O'Kane P, Pimenov A, Pokrovskii A, Rachinskii D and Zhezherun A 2009 *IEEE Control Systems Magazine* **29** 44–69

[25] Athukorallage B and Iyer R 2014 *Physica B: Condensed Matter* **435** 28 – 30 ISSN 0921-4526 9th International Symposium on Hysteresis Modeling and Micromagnetics (HMM 2013)

[26] Athukorallage B 2014 *Capillarity and Elastic Membrane Theory from an Energy Point of View* Ph.D. thesis Texas Tech University